



Article

In Silico Electrophysiological Investigation of Transient Receptor Potential Melastatin-4 Ion Channel Biophysics to Study Detrusor Overactivity

Chitaranjan Mahapatra ^{1,2,*} and Ravindra Thakkar ³

¹ Cardiovascular Research Institute, University of California San Francisco, San Francisco, CA 94158, USA

² Paris Saclay Institute of Neuroscience, 91440 Saclay, France

³ California Institute for Quantitative Biosciences, University of California Berkeley, Berkeley, CA 94720, USA; ravi.thakkar369@gmail.com

* Correspondence: cmahapatra97@gmail.com

Abstract: Enhanced electrical activity in detrusor smooth muscle (DSM) cells is a key factor in detrusor overactivity which causes overactive bladder pathological disorders. Transient receptor potential melastatin-4 (TRPM4) channels, which are calcium-activated cation channels, play a role in regulating DSM electrical activities. These channels likely contribute to depolarizing the DSM cell membrane, leading to bladder overactivity. Our research focuses on understanding TRPM4 channel function in the DSM cells of mice, using computational modeling. We aimed to create a detailed computational model of the TRPM4 channel based on existing electrophysiological data. We employed a modified Hodgkin-Huxley model with an incorporated TRP-like current to simulate action potential firing in response to current and synaptic stimulus inputs. Validation against experimental data showed close agreement with our simulations. Our model is the first to analyze the TRPM4 channel's role in DSM electrical activity, potentially revealing insights into bladder overactivity. In conclusion, TRPM4 channels are pivotal in regulating human DSM function, and TRPM4 channel inhibitors could be promising targets for treating overactive bladder.

Keywords: urinary incontinence; TRPM4 ion channel; action potential; computational modeling



Citation: Mahapatra, C.; Thakkar, R. In Silico Electrophysiological Investigation of Transient Receptor Potential Melastatin-4 Ion Channel Biophysics to Study Detrusor Overactivity. *Int. J. Mol. Sci.* **2024**, *25*, 6875. <https://doi.org/10.3390/ijms25136875>

Academic Editors:
Mohammad Shahidullah and Paul
James Donaldson

Received: 21 May 2024
Revised: 18 June 2024
Accepted: 20 June 2024
Published: 22 June 2024



Copyright: © 2024 by the authors. Licensee MDPI, Basel, Switzerland. This article is an open access article distributed under the terms and conditions of the Creative Commons Attribution (CC BY) license (<https://creativecommons.org/licenses/by/4.0/>).

1. Introduction

People encounter diverse health issues that influence their well-being. Experiencing a non-lethal heart attack can significantly alter one's perspective on life, prompting a heightened awareness of blood pressure, dietary modifications, the adoption of exercise regimens, decreased smoking, and various lifestyle adjustments. The gravity of a health ailment might not always be obvious but can profoundly affect one's quality of life. Many of us may overlook the simplicity of typical urinary bladder function. The primary physiological roles of a healthy urinary bladder are to store urine and facilitate voluntary micturition (the act of urinating) [1,2]. However, overactive bladder syndrome (OAB, also known as overactive detrusor function) presents symptoms such as urgency for urination with or without urge incontinence, frequent urination, and nocturia (waking at night to urinate) [3–8]. The impact of OAB on an individual's quality of life, on the healthcare system, and on the workforce carries considerable economic burdens [9–11]. The exact cause of OAB remains largely unknown. The detrusor smooth muscle (DSM) within the bladder wall plays a crucial role in bladder function [12,13]. During urine storage, DSM cells relax, allowing the bladder to hold urine for extended periods without leakage. When urination is necessary, DSM cells contract synchronously with the coordinated action of internal and external urethral sphincters [14,15]. This coordinated activity, orchestrated by the brain and spinal cord, triggers DSM contraction for micturition. In OAB, involuntary contractions of DSM cells can occur during urine storage, leading to leakage [16,17]. Lifestyle

changes and pharmacological therapy are among the strategies available to manage OAB and mitigate its complications [18,19]. Pharmacological therapy devoid of side effects is crucial in pathological situations to ensure optimal patient outcomes and minimize treatment-associated risks [20]. It allows for effective management of symptoms while preserving patient safety and quality of life. Treatment options for OAB often involve medications like anticholinergics and beta-3 adrenergic agonists, designed to alleviate symptoms by calming the DSM and lessening the urge to urinate frequently [21,22]. Nonetheless, these medications can lead to side effects such as dry mouth, constipation, blurred vision, and cognitive decline with anticholinergics, as well as potential hypertension with beta-3 adrenergic agonists [23–25]. Therefore, understanding the DSM electrophysiology becomes essential to explore new pharmacological targets to mitigate the side effects induced by conventional medications.

Several experimental studies have revealed that DSM cells, found in various species, including humans, exhibit enhanced spontaneous phasic contractions, contributing to the development of an overactive bladder [26,27]. The initiation of spontaneous phasic contractions is triggered by the generation of evoked spontaneous action potentials (APs) and accompanying calcium (Ca^{2+}) dynamics [28–31]. A thorough biophysical explanation of DSM AP generation is crucial for comprehending spontaneous contractions and for exploring novel pharmacological targets for overactive bladder treatment. The electrical activities in all excitable tissues are regulated by the influx and efflux of charged ions through a network of ion channels situated at the cell membrane. In a resting state, electrically excitable cells maintain a specific resting membrane potential, which varies among different tissue types, including neuronal cells, cardiac cells, and smooth muscle cells. A transient rise in cytoplasmic calcium $[\text{Ca}^{2+}]_i$ is an important reason behind DSM cell contraction [32,33]. The influx of extracellular Ca^{2+} ions occurs mainly via voltage-dependent L-type and T-type Ca^{2+} channels [34–36]. The sarco/endoplasmic reticulum (SR) is the principal Ca^{2+} store participating in the initial rapid increase in $[\text{Ca}^{2+}]_i$ by supplying Ca^{2+} via Ca^{2+} release mechanism by SR [37–39]. T-type Ca^{2+} channels are activated to depolarize the membrane potential until reaching the threshold potential, which then triggers the opening of L-type Ca^{2+} channels. Ca^{2+} influx via the L-type Ca^{2+} channel is essential for the rising phase of the DSM action potential, whereas various potassium (K^+) channels mediate the repolarization and, afterwards, a hyper-polarization period of the action potential, respectively [34,40–42]. Of the large family of mammalian K^+ channels, the Ca^{2+} -dependent K^+ channel, voltage-dependent K^+ channel, and the delayed rectifier K^+ channel are incorporated along with L-type and T-type Ca^{2+} channels in AP generation [41–44]. In addition, the Ca^{2+} -dependent K^+ channels in DSM cells are categorized into large (BK), intermediate (IK), and small (SK) conductance ion channels [45–48]. Several research groups have recently conducted an intriguing study revealing a novel regulatory mechanism of the transient receptor potential melastatin 4 (TRPM4) ion channel in modulating DSM cell excitability [49,50]. The TRPM4 channel has been shown to play a crucial role in regulating the resting membrane potential and basal tone of various smooth muscle cells. Through the utilization of the whole-cell voltage clamp method, researchers have successfully recorded TRPM4 channel currents in single smooth muscle cells within urinary bladder tissues from diverse animal subjects [49,51–56]. Their findings suggest that TRPM4 could serve as a novel therapeutic target for alleviating symptoms of OAB.

TRPM4 functions as a Ca^{2+} -activated non-selective cation channel, inducing cell membrane depolarization via sodium (Na^+) or K^+ entry and subsequent activation of L-type Ca^{2+} channels (Figure 1) [54]. In one study, the application of 9-phenanthrol resulted in hyperpolarization of DSM cell membranes, indicating the first evidence of TRPM4 regulation of human DSM cell resting membrane potential [55]. Moving forward, the researchers conducted *in vitro* experiments to investigate the impact of TRPM4 on spontaneous and phasic contractions of human DSM isolated strips. Inhibition of TRPM4 channels with 9-phenanthrol significantly reduced spontaneous and phasic contraction amplitude, muscle force integrality, contraction duration, contraction frequency, and muscle tone of the

DSM, highlighting TRPM4's critical role in human DSM modulation under physiological conditions. The illustration in Figure 1 explains the possible associated TRPM4 ion channel activation mechanism in DSM cells. Acetylcholine (Ach), a muscarinic agent, activates the muscarinic receptors (M3) at the membrane [57–59]. Then, phospholipase C (PLC) is activated, leading to the hydrolysis of phosphatidylinositol 4,5-bisphosphate (PIP2) into inositol trisphosphate (IP3) and diacylglycerol (DAG). IP3 then binds to IP3 receptors on the sarcoplasmic reticulum (SR), causing the release of Ca^{2+} ions from the SR stores into the cytoplasm [53,60]. One portion of the elevated $[\text{Ca}^{2+}]_i$ activates the TRPM4 ion channel and allows the influx of Na^+ ions (or K^+ ions) to depolarize the membrane. When the depolarization crosses the threshold potential, the L-type Ca^{2+} channel, which is a voltage-dependent calcium channel (VDCC), opens and allows an influx of extracellular Ca^{2+} into the cytoplasm. The cytoplasmic Ca^{2+} , released from the SR store and via the L-type Ca^{2+} channel, triggers contraction after the generation of the action potential.

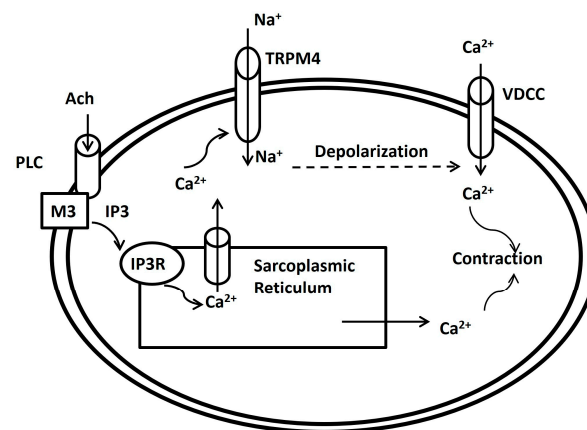


Figure 1. Schematic illustration of the proposed physiological role for TRPM4 channels in DSM cells. According to the postulated mechanism, the TRPM4 channels via sarcoplasmic reticulum Ca^{2+} -dependent activation participate in a positive feedback loop to maximize DSM contractility by providing Na^+ -depolarizing conductance.

Unfortunately, the quantitative description of the modulatory effects of the TRPM4 ion channel on DSM cell electrical properties has not been thoroughly explored due to the highly complex nature of the experimental procedures involved in DSM cell electrophysiology. Unlike cardiac and neuronal electrophysiological studies, obtaining comprehensive electrical recordings from smooth muscle cells is challenging. Consequently, most research focuses on the TRPM4 channel's impact on DSM contraction, rather than on its effect on passive or active electrical properties, like spike/AP modulation. Understanding the biophysical parameters governing DSM cell electrophysiology is crucial for drug design accuracy. Additionally, there is debate over variations in inward and outward currents in DSM electrophysiology. The redundancy of ion channel types regulates cellular functions and maintains physiological balance, ensuring resilience against perturbations [61]. However, investigations of the redundancy and resilience of TRPM4 concerning other inward current ion channels in DSM cells remain unexplored.

Over the past few decades, computational and mathematical modeling techniques have enhanced our comprehension of intricate biological processes. By simulating diverse scenarios and predicting outcomes, these methods offer insights that may be challenging to attain through traditional experimental approaches [62]. The primary goal of computational biophysical modeling is to provide insights into the structure, function, and dynamics of biological systems that may be difficult or impossible to obtain through experimental methods alone. In the realm of smooth muscle electrophysiology, computational simulations have been instrumental in exploring cellular biophysics and in modulating cellular electrical activities. These models shed light on ion channel function, encompassing aspects such as conductance, ion selectivity, and channel opening, which hold significance

in pathological conditions. Moreover, biophysical modeling directly simulates ion flux through membrane channels, facilitating a deeper understanding of their behavior and their involvement in disease processes. While computational models for various types of smooth muscle cells, such as intestinal [63], uterine [64–66], ureter [67–69], jejunal [70], vas deferens [71–74], gastric [75,76], mesenteric [77], small bowel [78], urethra [79,80], and arterial [81] smooth muscle cells, have been developed, models for DSM cells are relatively underdeveloped. The models published on DSM electrophysiology have yet to explore the modulatory properties of TRPM4 ion channels in DSP action potentials [82–88]. The present *in silico* model aims to elucidate the biophysical mechanisms underlying DSM electrophysiology, and to investigate the impact of the TRPM4 ion channel on the firing rate of DSM action potentials. Our objectives in developing this model are threefold. Firstly, leveraging experimental data, we will simulate and validate the kinetics of TRPM4 ion channels in response to changes in intracellular Ca^{2+} concentration. Secondly, we will integrate these ion channels into a single-compartment biophysical DSM model to simulate APs and explore alterations in AP parameters associated with TRPM4 ion channel activation. Lastly, we seek to derive novel biological insights to corroborate existing hypotheses drawn from various experiments, and propose new hypotheses for future research endeavors.

2. Results

The TRPM4 channel's current behavior is modeled and simulated based on Equations (8)–(10), following the principles of the Hodgkin–Huxley (HH) formalism, which incorporates activation and inactivation parameters. The equilibrium potential of TRPM4, denoted as E_{Na} , is set at -40 mV. Activation parameters are computed across varying intracellular Ca^{2+} concentrations (Cai), with a baseline Cai concentration of 0.1 mM during rest. In Figure 2, we present the steady-state activation curves for the TRPM4 channel, comparing our model's simulated curve (depicted by the solid red line) with experimental data (shown as filled triangles) sourced from Demion et al. (2007) [89]. The steady-state activation curve is unitless and ranges between 0 and 1. The x-axis is the logarithmic value of the Cai value. The comparison demonstrates a close alignment between our simulated curve and the experimental data. Notably, higher concentrations of Cai correspond to increased steady-state activation values, indicating an augmented TRPM4 current.

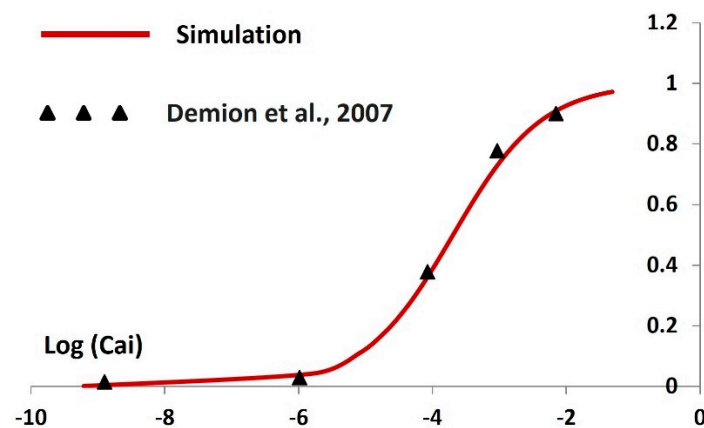


Figure 2. Simulated steady-state activation curve showing $\log(\text{Cai})$. The solid line represents the result from simulation, where the solid filled triangle shows the adapted experimental data from Demion et al., 2007 [89].

Subsequently, we integrated the TRPM4 channel into a single-compartment DSM model, as outlined by [83]. Earlier sections of this paper have detailed the inclusion of various ion channels within the DSM model. Before introducing the TRPM4 channel, we meticulously evaluated the stability, robustness, and flexibility of the DSM cell model, adhering to the methodologies outlined in the Section 4. Minor adjustments were made to certain parameters (particularly to ion channel conductances and time constant values) to

ensure the stability of the resting membrane potential. The resting intracellular calcium concentration was maintained at 150 nM. Table 1 provides a comprehensive list of all ion channels incorporated into the model, along with their respective maximum conductances necessary for maintaining the stable resting membrane potential.

Table 1. Maximum conductances of ion channels.

Ion Channel	Conductance (S/cm ²)
T-type Ca ²⁺ channel	0.0002
L-type Ca ²⁺ channel	0.0003
Voltage-gated K ⁺ channel-Kv1	0.0006
Voltage-gated K ⁺ channel-KDR	0.0009
Calcium-dependent K ⁺ channel (BK)	0.0008
Calcium-dependent K ⁺ channel (IK)	0.0007
Calcium-dependent K ⁺ channel (SK)	0.0001
ATP-dependent K ⁺ channel	0.0001
Inward-rectifying channel	0.0001
TRPM4 Channel	0.0002

By incorporating all ion channel models, including TRPM4, our primary aim was to uphold a physiological resting membrane potential (RMP) of -52 mV. The model's robustness was confirmed by maintaining the RMP at -52 mV for 2000 ms, as illustrated in Figure 3. However, at the outset (0 ms), the model experienced a brief period of instability due to the behavior of all ion channels, resulting in slight fluctuations in membrane potential (Figure 3a). To address this, the time scale (x-axis) in Figure 3b begins from 500 ms onwards, excluding these initial fluctuations.

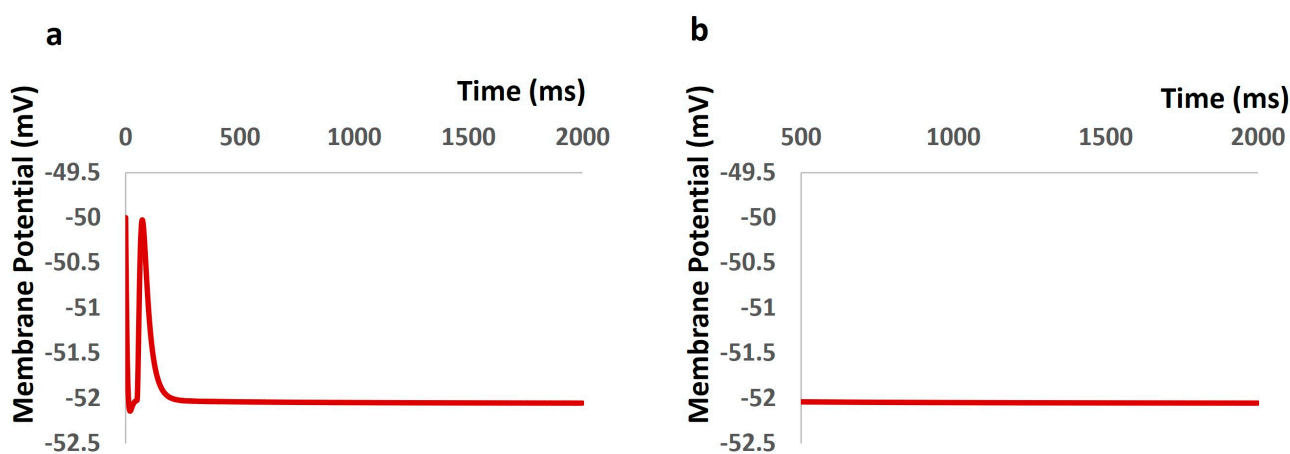


Figure 3. DSM model showing initial fluctuation (a) and constant resting membrane potential maintained at -52 mV (b).

We administered current stimuli with varying amplitudes lasting 10 ms to investigate evoked depolarization, action potential (AP) generation, and threshold estimation. No spikes occurred until the stimulus reached 0.56 mA, at which point the AP was triggered (Figure 4a). Analysis of the AP (depicted by the solid red line) and depolarization (represented by the dashed red line) facilitated the prediction of the threshold required to initiate the AP, estimated at -38.56 mV. Subsequently, we introduced synaptic input with different amplitudes to study evoked depolarization, AP generation, and threshold prediction. No spikes were observed with a stimulus of 0.0078 μ S, while an AP was elicited with a stimulus of 0.0079 μ S. Analysis of the simulated AP (depicted by the solid red line) and depolarization (shown as the dashed red line) predicted the threshold for AP initiation at -38.42 mV. Experimental data on AP in mice's DSM cells under synaptic stimulus, as reported by [83], were compared with our model-simulated AP. The extracted data from

this experimental AP (illustrated by the dashed blue line) exhibited a close match with our model's output, corroborating the accuracy of our model.

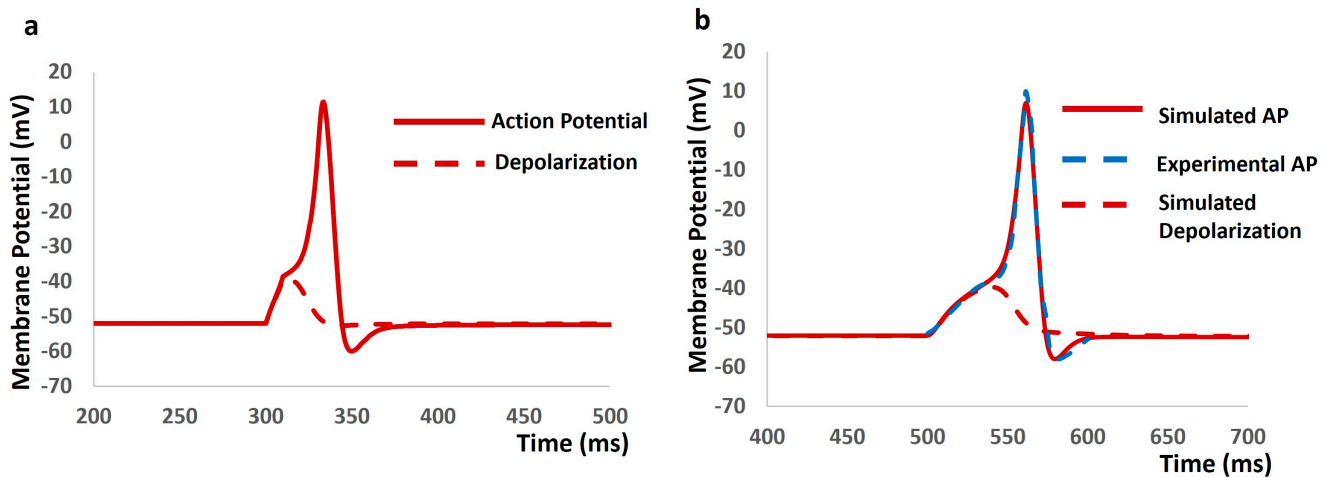


Figure 4. (a) The model generated AP (solid red line) and depolarization (dashed red line) with the current stimulus. (b) The model generated AP (solid red line), experimental AP (solid blue line), and simulated depolarization (dashed red line) with synaptic input stimulus.

Our subsequent investigation aimed to explore the modulatory impact of the TRPM4 channel on the electrical characteristics of the DSM cell. It is important to highlight one of the most intriguing aspects of DSM cell action potential generation, namely the variability in action potential shapes. Unlike neuronal and cardiac cells, which typically exhibit uniform action potentials for a given cell type, isolated DSM cells can produce various types of action potentials. These variations stem from differences in action potential duration, the shape of depolarizing and repolarizing phases, after-depolarization potential, and after-hyperpolarizations. Figure 5 depicts one type of DSM action potential following a 10% and 20% increase in the maximum conductance of the TRPM4 ion channel. The action potential represented by the solid red line arises after a 10% increase in the maximum conductance of the TRPM4 ion channel. Notably, the resting membrane potential becomes more positive following action potential generation. However, this generated action potential aligns with physiological expectations. In contrast, the action potential depicted by the solid black line emerges after a 20% increase in the maximum conductance of the TRPM4 ion channel. Although an action potential is generated, this particular type of action potential does not match physiological norms. Elevated conductance of the TRPM4 channel induces model instability.

To conduct a more comprehensive quantitative examination, we performed sensitivity analysis on the TRPM4 conductance concerning action potential parameters. Figure 6 illustrates the alterations in action potential parameters, specifically the resting membrane potential (solid red line) and action potential duration (dashed-dotted red line), in response to variations in the maximum conductance of the TRPM4 channel. All parameters were normalized for enhanced clarity. It is noteworthy that each action potential parameter fluctuates within a range of up to +20% and −30%, indicating the stability of the action potential across the range of TRPM4 channel conductance.

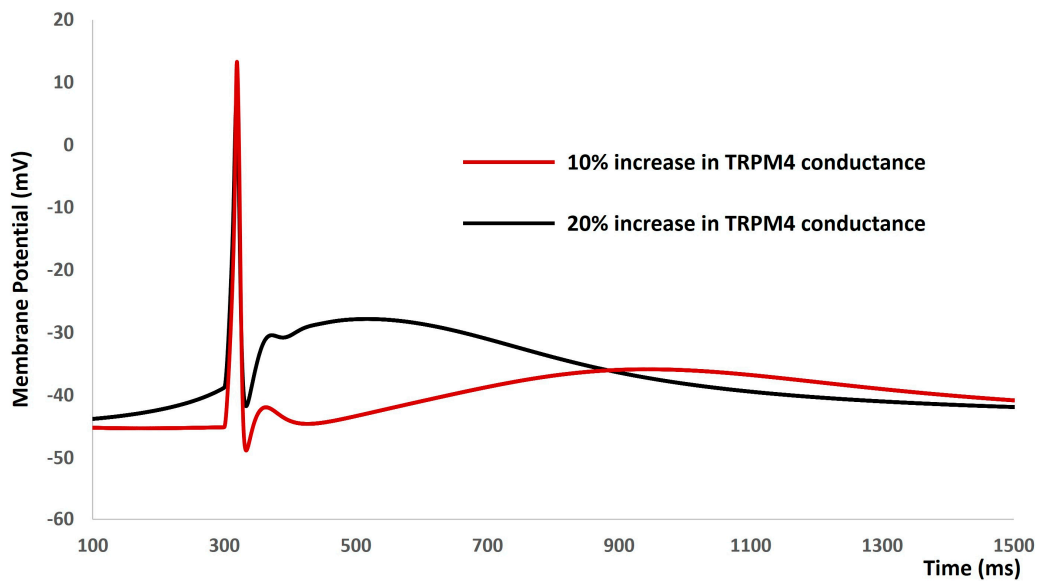


Figure 5. DSM action potential after a 10% (solid red line) and 20% (solid black line) increase in the maximum conductance of the TRPM4 ion channel.

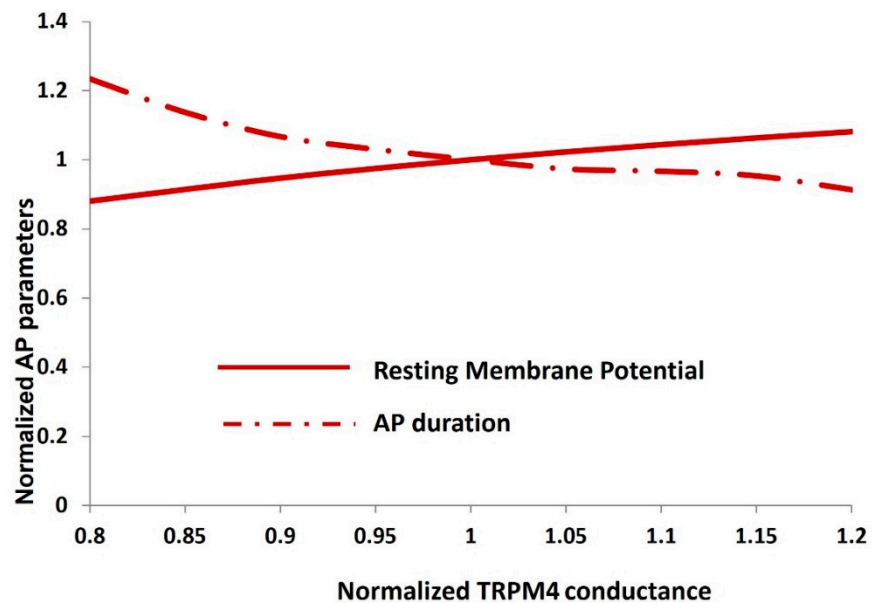


Figure 6. Sensitivity analysis of the TRPM4 channel conductance for DSM resting membrane potential and action potential duration.

The prevalence of ion channels in excitable cells (such as neurons, cardiac cells, and muscle cells) prompts fundamental inquiries into how the unique intrinsic characteristics of individual cells arise from their specific complement of channels. Across all excitable cells, many ion channels exhibit overlapping voltage and time-dependent traits. We propose that these shared properties contribute to the robustness of physiological function. Despite displaying consistent and similar behaviors, individual excitable cells of the same type demonstrate variability in ion channel conductance densities [61,90]. This complexity complicates the direct function assignment to any particular conductance, and is associated with the diverse responses of similar cells to disturbances, deletions, and pharmacological treatments. Several experimental investigations have shown that the activation of the T-type Ca^{2+} channel depolarizes the DSM cell to the threshold of the L-type Ca^{2+} channel, for which the cell generates AP [91]. To examine our hypothesis concerning a mutation in the T-type Ca^{2+} channel (whereby the maximum conductance of the T-type Ca^{2+} channel is set to zero),

we adjusted the conductance of the TRPM4 channel to maintain the electrophysiological behavior of the DSM cell. As illustrated in Figure 7, when the T-type Ca^{2+} channel was muted (depicted by the dashed red line), the DSM cell failed to generate any action potential. Further adjustments to the parameters of the TRPM4 channel rendered the DSM cell incapable of generating action potentials. However, by fine-tuning the parameters of the TRPM4, L-type Ca^{2+} channel, and inward rectifying channel, the DSM cell was able to generate action potentials without the presence of the T-type Ca^{2+} channel (depicted by the solid red line). Initially, the model exhibited stochastic behaviors, but subsequent adjustments to other ion channel parameters enabled the generation of action potentials. This finding strongly supports the variability and resilience of our computational model. It should be noted that other ion channel blockers were applied in the DSM models, and their effects on AP were shown in [83].

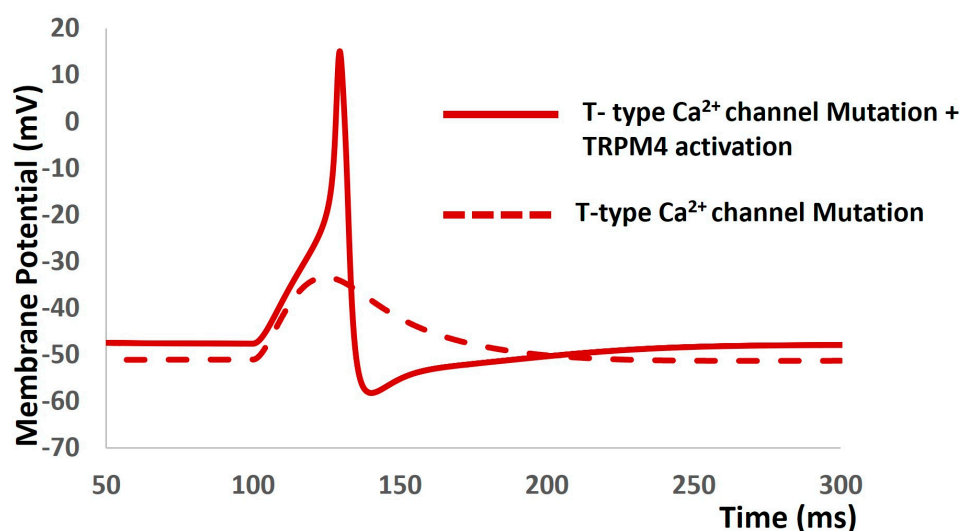


Figure 7. DSM cell generates action potential (solid red line) with mutation of T-type Ca^{2+} channel. The dashed line depicts the absence of action potential.

3. Discussion

OAB syndrome has a profound impact on people's lives, and poses significant financial challenges. This condition, characterized by sudden and uncontrollable urges to urinate, often results in frequent bathroom visits, disrupted sleep, and limitations in daily activities. The anxiety and embarrassment surrounding potential accidents can lead to social isolation and reduced productivity. Additionally, managing OAB requires ongoing medical expenses, such as doctor visits, medication, and possibly surgery, which places strain on both personal finances and healthcare systems. Despite its widespread occurrence and consequences, much remains unknown about the underlying causes and effective treatments for OAB. Fundamental research plays a crucial role in unraveling the complexities of this condition, including understanding the neural pathways involved in bladder control, identifying early detection biomarkers, and developing targeted therapies with minimal side effects. DSM contraction is closely linked to OAB syndrome [16,17], as heightened activity in these muscles can lead to involuntary and frequent bladder contractions, resulting in the characteristic urgency and urge incontinence experienced by individuals with OAB. A thorough exploration of the underlying biophysical mechanisms behind DSM electrophysiology is crucial for identifying new pharmacological targets with minimal side effects. As a mechanical event, the contraction is initiated by intracellular calcium elevation and the generation of action potential. Ion channels play a crucial role in modulating the underlying electrical properties, including the action potential, across the DSM cell membrane. Hence, accurately quantifying the individual ion channel's contribution to modulating the action potential will aid the exploration of more effective drugs for overactive bladder treatment. In recent years, multiple experimental findings have indicated the presence of

the TRPM4 ion channel in DSM cells and its role in modulating DSM contraction [49,50]. Due to the highly complex nature of experimental smooth muscle electrophysiology setups, the quantified contribution of the TRPM4 channel to DSM cell membrane potential and action potential has not yet been studied.

Computational and *in silico* approaches have revolutionized the field of electrophysiology by providing valuable insights into the behavior of ion channels at a fundamental level. These methods simulate the complex interactions of ion channels with high precision, allowing researchers to explore diverse scenarios and predict ion channel behavior under different conditions. By complementing experimental studies, computational models enhance our understanding of ion channel function, kinetics, and pharmacology. Moreover, they offer a platform for hypothesis testing and guide experimental design, ultimately accelerating the discovery of novel targets and therapies for various physiological and pathological conditions. While numerous computational models have been published regarding DSM cell electrophysiology, none of them has incorporated the TRPM4 channel for investigation [82–84,86,87]. Computational modeling is an ongoing process, wherein established models are continuously refined, with new experimental findings yielding more fruitful research outcomes. To the best of our knowledge, the model presented by us is the first biophysically constrained DSM cell model to investigate the contribution of the TRPM4 channel to DSM cell excitability.

Our first objective in developing this model was to employ differential equations, Hodgkin–Huxley formalisms, and parameters to accurately replicate the internal kinetics of the TRPM4 channel. We have depicted the simulated steady-state activation curve across various calcium concentrations (Figure 2). Validation against experimental data reinforces the heightened accuracy of our TRPM4 ion channel model, confirming the successful achievement of our first objective. Our second objective was to integrate the TRPM4 channel into a DSM cell model and examine its modulating effects on cellular excitability. Before integrating the new TRPM4 channel, we validated the previous model to ensure its robustness and reproducibility. Once we confirmed the proper functioning of the model, we proceeded with the integration of the TRPM4 channel. However, adding a foreign element to an established model often results in aberrant stochastic behavior. Similarly, our model exhibited instability after the incorporation of the TRPM4 channel. To address this, we carefully adjusted the maximum conductances of ion channels to stabilize the model and replicate previously simulated outputs. We validated the simulated synaptic potentials and action potentials by comparing them with experimental data, confirming our model's ability to replicate experimental findings [83] (Figure 4). Subsequently, we adjusted the maximum conductance of the TRPM4 channel within physiological ranges to assess its impact on the resting membrane potential, action potential threshold, and peak amplitude. Activation of the TRPM4 channel leads to a shift in the resting membrane potential towards a more positive state, reduces the threshold potential for action potential initiation, and increases the peak amplitude of the action potential. This suggests that overexpression of TRPM4 channels across the DSM cell membrane could induce heightened spontaneous contractions, a primary symptom of overactive bladder [49,50]. Therefore, controlled doses of TRPM4 channel blockers may mitigate this pathological condition. Conversely, in absence of overexpressed channels, their inherent activity may still lead to overactivity due to spontaneous intracellular calcium elevation. Experimental studies have demonstrated transient increases in intracellular calcium, such as calcium sparks, puffs, and waves [92], which could activate TRPM4 channels locally, exacerbating overactive bladder symptoms. The term “localization” distinguishes TRPM4 channel activation from calcium-dependent potassium channel activation, which hyperpolarizes the membrane, reducing cellular excitability. To further validate our model, we conducted a sensitivity analysis, providing additional quantitative insights into how the TRPM4 channel influences cellular electrical properties. As a primary goal of any computational physiology model is to generate new hypotheses, our third objective was to propose novel insights into the TRPM4 channel in detrusor muscle biophysics. In the introduction, we briefly discussed

the redundancy of ion channel types to ensure resilience against perturbations. Building on this concept, we inactivated the T-type calcium channel by reducing its maximum conductance to zero, then simulated all electrical properties by adjusting conductances and other parameters for the remaining ion channels. This revealed that the TRPM4 channel could compensate for the absence of the T-type calcium channel. Our hypothesis suggests that the TRPM4 channel may serve as a standby ion channel to maintain bladder physiology in cases of dysfunction or mutation in the T-type calcium channel.

Computational models inherently have several limitations. Firstly, our current model investigated the modulating effects of TRPM4 channels on spike-type action potentials in the DSM model. However, DSM cells also generate pacemaking-type action potentials, which are not simulated in this model. To date, no biophysically detailed DSM model has been developed to simulate pacemaking action potentials. Additionally, most of the experimental research papers highlighted the spike-type action potentials in single isolated DSM cells [82,83]. Although the action potential was validated against experimental data from mice's urinary bladders, our ion channel parameters were derived from other animals (mice and guinea pigs) and organs, due to a lack of specific data [82,83]. Additionally, while actual smooth muscle morphology may not perfectly align with a cylindrical shape, our model is designed based on this simplified geometry. Furthermore, DSM cells function as a syncytium, where multiple cells are interconnected via gap junctions, enabling electrical signal propagation. However, our model is limited to a single-compartment isolated cell. Future model expansions could involve investigating the effects of TRPM4 channel modulation in multicompartmental tissues with complex calcium dynamics.

4. Materials and Methods

4.1. Model Adaptation

Biophysically detailed cell modeling for neuronal cells made its debut in 1952 in neuroscience, thanks to the groundbreaking work of Hodgkin and Huxley on the squid giant axon [93]. In the 1960s, Noble pioneered the first models of cardiac cellular activity [94]. Since then, an impressive array of mathematical models for neuronal cells, cardiac muscle, and smooth muscle electrophysiology have emerged. The complexity of these models has steadily increased over the years as more experimental data have become available. Several DSM cell electrophysiology models have been mathematically designed to mimic the behavior of DSM electrical activities [82–84,86,87]. These models also serve as a bridge between cellular-level models and tissue-level function, offering a comprehensive understanding of DSM cell electrical activity across different scales. For establishing a single-compartment DSM AP model to integrate the TRPM4 ion channel, we have adapted the model [83] for simulating DSM cell electrical properties. The DSM cell membrane's cylindrical single-cell morphology and passive electrical properties are derived from the experimental data for a single isolated DSM cell [95]. The length, diameter, membrane resistivity, cytoplasmic resistivity, and membrane capacitance are 200 μm , 6 μm , 138 $\text{k}\Omega\cdot\text{cm}^2$, 183 $\Omega\cdot\text{cm}$, and 1 $\mu\text{F}/\text{cm}^2$ respectively.

4.2. General Membrane Current Descriptions

The DSM cell is electrically defined by a resistor–capacitor (RC) circuit, where the membrane capacitance C_m is parallel with the variable ion channel conductance g_{ion} . All active ion channel conductances g_{ion} are associated with respective Nernst potential E_{ion} in series. Figure 8 illustrates the schematic overview of the parallel conductance model for ionic current (I_{ion}), and it shows the flow of ion 'X⁺' under the influence of an electrochemical driving force.

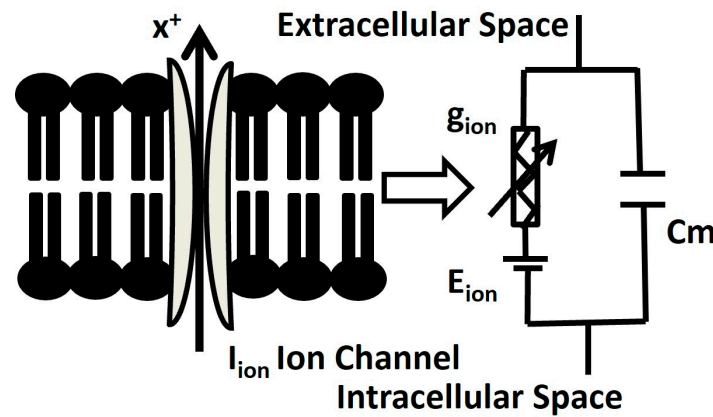


Figure 8. Schematic overview of parallel conductance model for ionic current. Further elucidation is provided in the subsequent paragraph.

The calculation of the individual ionic current follows the principles of Ohm’s law, traditionally expressed through Equation (1).

$$I_{ion} = \bar{g} [m(V_m, t, [Ca^{2+}]_i)]^x [h(V_m, t, [Ca^{2+}]_i)]^y (V_m - E_{Nernst}) \quad (1)$$

In Equation (1), \bar{g} and E_{Nernst} represent the maximum channel conductance and Nernst potential specific to the ion channel under consideration. The variable parameters m and h correspond to dimensionless activation- and inactivation-gating variables, respectively, which are dependent on time, voltage, and Ca^{2+} concentration. To facilitate equation fitting, an additional pair of dimensionless parameters denoted as ‘ x ’ and ‘ y ’ are introduced, determined through a system of first-order differential equations, following the classical Hodgkin–Huxley (HH) formulation mechanisms [93].

For example, Equation (2) computes the instantaneous value of the activation variable “ m ” in our DSM cell model.

$$\frac{dm(V_m, t)}{dt} = \frac{m_{\infty}(V_m) - m(V_m, t)}{\tau_m} \quad (2)$$

In this equation, m_{∞} represents the steady-state value, and τ_m denotes the time constant, both of which are functions of voltage and/or ionic concentrations.

In this context, the relationship between the state parameter and the membrane potential (V_m) for ion channels is elucidated through the Boltzmann equation.

$$m_{\infty} = 1 / (1 + \exp((V_m + V_{m\frac{1}{2}}) / S_m)) \quad (3)$$

where $V_{1/2}$ is the half activation potential and S is the slope factor.

The large conductance calcium-activated potassium (BK) channel kinetics have been elucidated through a multi-state Markov model (MM) [96], which offers a detailed representation of the channel’s sensitivity to Ca^{2+} , enhancing precision. Figure 9 illustrates the schematic diagram of the 10-state Markov model for the BK channel. The MM model enhances the accuracy of the description of a multi-agent activated ion channel by incorporating multiple closed and open states to represent its internal conditions. This model comprises closed states denoted as C0, C1, C2, C3, and C4, and five corresponding open states denoted as O0, O1, O2, O3, and O4. Among these, the open state O4 facilitates the passage of K^+ ions via BK channels driven by the instantaneous electrochemical driving force (EDF). The BK current (I_{BK}) is determined using the following equation:

$$I_{BK} = \overline{g_{BK}} \times O \times (V - E_K) \quad (4)$$

where $\overline{g_{BK}}$ is the maximum conductance and O is the summation of O1, O2, O3, and O4.

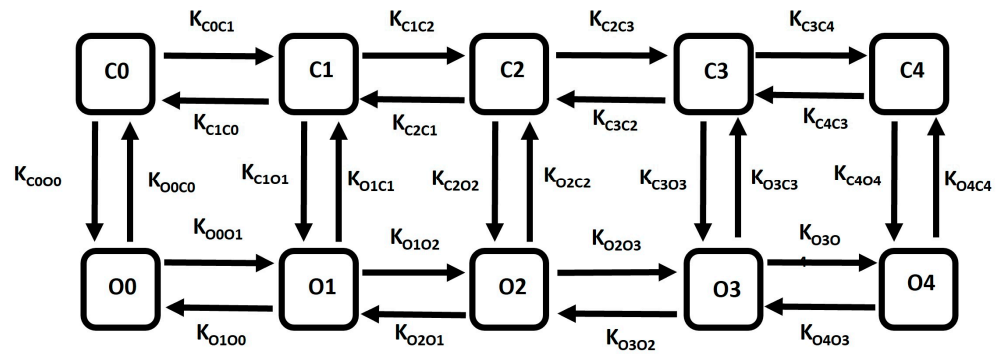


Figure 9. Schematic diagram of 10-state Markov model for BK channel. A detailed explanation is provided in the text.

Common rate equations:

$$K_{on} = 335, K_{coff} = 26, K_{off} = 26, O = O1 + O2 + O3 + O4 \tag{5}$$

Rate equations for voltage-dependent transitions:

$$K_{C0O0} = 0.03162 \times a, K_{C1O1} = 0.000969 \times a, K_{C2O2} = 0.0000381 \times a, K_{C3O3} = 0.000881 \times a, K_{C4O4} = 0.054324 \times a, K_{O0C0} = 328.1084 \times b, K_{O1C1} = 154.1736 \times b, K_{O2C2} = 33.6594 \times b, K_{O3C3} = 0.097312 \times b, K_{O4C4} = 0.000406 \times b \times cai \tag{6}$$

State equations for calcium (cai)-dependent transitions:

$$\begin{aligned} K_{C0C1} &= 3 \times K_{on} \times cai, K_{C1C2} = 4 \times K_{on} \times cai, K_{C2C3} = 3 \times K_{on} \times cai, K_{C3C4} = K_{on} \times cai \\ K_{C4C3} &= 3 \times K_{coff} \times cai, K_{C3C2} = 4 \times K_{coff} \times cai, K_{C2C1} = 3 \times K_{coff} \times cai, K_{C1C0} = K_{coff} \times cai \\ K_{O0O1} &= 3 \times K_{on} \times cai, K_{O1O2} = 4 \times K_{on} \times cai, K_{O2O3} = 3 \times K_{on} \times cai, K_{O3O4} = K_{on} \times cai \\ K_{O4O3} &= 3 \times K_{off} \times cai, K_{O3O2} = 4 \times K_{off} \times cai, K_{O2O1} = 3 \times K_{off} \times cai, K_{O1O0} = K_{off} \times cai \end{aligned} \tag{7}$$

In Equations (5)–(7), the parameter values are defined to obtain the most accurate model of the BK ion channel, aiming to simulate the current–voltage relationship curve and the BK current under different membrane potentials and internal Ca²⁺ concentration.

4.3. TRPM 4 Channel with Ca²⁺ Sensing Mechanism

Here, the mathematical interpretation of the TRPM4 ion channel is based on conventional Hodgkin–Huxley formalism. In this model, Hodgkin–Huxley formalism is adapted for I_{Na} ionic currents in Equation (8):

$$I = \bar{g}zm^x(V_m - E_{rev}) \tag{8}$$

where \bar{g} is maximum conductance, E_{rev} is Nernst potential for sodium ion, m is intracellular calcium concentration-dependent activation variable, and x is the power for the gating variable.

The first-order differential equation is used in Equation (9) to describe the time and calcium-dependent nature of gating variable m :

$$\frac{dm}{dt} = \frac{(m_{\infty} - m)}{\tau_m} \tag{9}$$

where m_{∞} and τ_m are defined as the steady-state value and time constant of gating variable ‘ m ’ respectively.

Here the activation steady state is expressed by the Hills equation:

$$z_{\infty} = 1 / (1 + \left(\frac{Cah}{Cai}\right)^n) \tag{10}$$

where Cah is half inhibition intracellular calcium ion centration, Cai is free calcium concentration, and n is the Hill coefficient. All modeling parameters are borrowed from literature based on experimental studies. Cah and n are fitted to match with the experimental result.

4.4. Whole DSM Cell Model and Simulation

Figure 10 shows the list of active ion channels incorporated into our DSM cell. In our model, the two types of voltage-gated Ca²⁺ channels are T-type (I_{CaT}) and L-type (I_{CaL}) Ca²⁺ channels.

Voltage-gated K^+ channels are inward-rectifying channels (I_{KIR}), delayed rectifier channels (I_{KDR}), and fast (I_{Kv1}) channels. Ca^{2+} -activated K^+ channels are large conductance (I_{BKCa}), intermediate conductance (I_{IKCa}), and small conductance (I_{SKCa}) channels. The TRPM4 channel (I_{TRPM4}) and leakage channels (I_l) have also been added to this single-compartment DSM cell model.

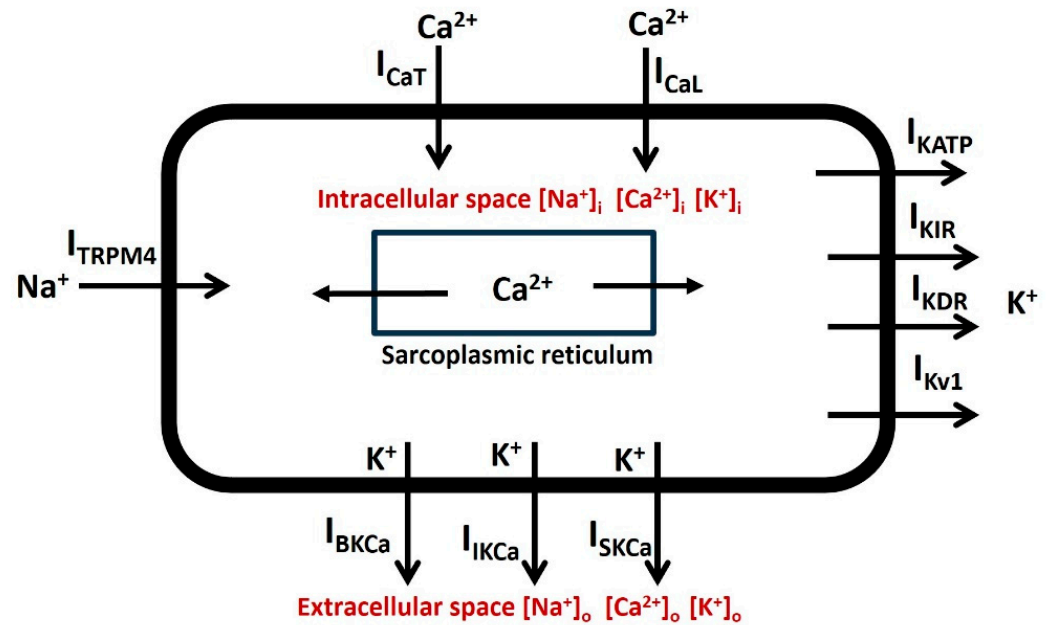


Figure 10. Schematic diagram illustrating all ionic components within a DSM cell. The accompanying paragraph provides descriptions for each component.

The synaptic input defined by the alpha function [97] or a brief square pulse of injected current (variable duration and magnitude) serves as the external stimulus to generate action potentials in the whole-cell model. Subsequently, the conductance is adjusted to explore the modified response in action potentials and resting membrane potential. Simulations were conducted on a PC equipped with an Intel Core i7 CPU operating at 3.80 GHz and with a dual-core setup. The NEURON simulation environment was utilized for model creation, renowned for its accurate portrayal of excitable cells [98]. While NEURON primarily employs implicit integration techniques, like backward Euler and a variant of Crank-Nicolson for stability, it also supports Euler's method due to its efficiency and minimal memory usage [99]. In NEURON, the actual simulation time, t , is measured in milliseconds, and at each time step it is incremented by dt . A smaller dt is required for more accurate results. The simulation speed depends on the complexity and modeling approaches used for the network. To balance simulation speed and accuracy, we set dt to 0.04 ms. We also adapted NEURON's multiple run fitter optimization algorithms to optimize our running fitness for action potential generation. This process usually entails scrutinizing different aspects of our running performance and leveraging the gathered data to refine our training routine, aiming for improved outcomes.

Following model creation, stability and consistency were evaluated by adjusting the maximum conductance (g_{max}) of ionic conductances within $\pm 30\%$ of the default value. Results demonstrated stable action potentials exhibiting anticipated responses to changes in conductance; for instance, increased g_{max} led to higher AP peak amplitudes while preserving the AP's normal characteristics. The experimental data used for validation in our current model are borrowed from a previously published paper from 2018 [83], which involved a collaboration for obtaining experimental data recordings. Goodness-of-fit (GoF) involves assessing how well the observed data align with the data predicted by a model, typically through a fit statistic or measure of deviation, such as residuals, Chi-square, or deviance. The standard error of the regression (S) or root mean squared error (RMSE) serves as a measure of GoF in our analyses of simulated action potentials, chosen due to the inadequacy of R^2 for nonlinear comparisons [100]. S is computed using the following formula:

$$S = \sqrt{\frac{\sum (Y_{Exp} - Y_{Sim})^2}{M - N}} \quad (11)$$

In Equation (11), Y_{expt} represents the experimental value, Y_{sim} denotes the corresponding simulated fit value, N stands for the number of parameters utilized in the fitting equation, and M represents the total number of data points. A smaller S value indicates lower average errors and indicates a better fit. We established a threshold for a satisfactory model as 5% of the difference between the maximum and minimum values observed in the experimental data. Any S value below this threshold is deemed indicative of a good fit.

The model code will be accessible on GitHub and the repository (<https://modeldb.science>, accessed on 5 May 2024) for open-source code sharing.

Author Contributions: C.M. conceived the idea of the draft, and wrote the manuscript. R.T. also helped with the writing, editing, and formatting of the final draft. C.M. also responded to reviewers' comments. All authors have read and agreed to the published version of the manuscript.

Funding: This research received no external funding.

Institutional Review Board Statement: Not applicable.

Informed Consent Statement: Not applicable.

Data Availability Statement: Data are contained within the article.

Acknowledgments: Chitaranjan Mahapatra is thankful to UCSF, San Francisco for providing space and other required facilities for the completion of this manuscript. R.T. is thankful to UC Berkeley for providing facilities and space for the completion of the manuscript.

Conflicts of Interest: The authors declare no conflicts of interest.

References

1. de Groat, W.C.; Yoshimura, N.A. Anatomy and physiology of the lower urinary tract. *Handb. Clin. Neurol.* **2015**, *130*, 61–108. [[PubMed](#)]
2. Tyagi, S.; Tyagi, P.; Yoshimura, N.; Chancellor, M.B. Physiology of micturition. In *Textbook of Female Urology and Urogynecology—Two-Volume Set*; CRC Press: Boca Raton, FL, USA, 2017; pp. 232–246.
3. Abrams, P. Describing bladder storage function: Overactive bladder syndrome and detrusor overactivity. *Urology* **2003**, *62*, 28–37. [[CrossRef](#)] [[PubMed](#)]
4. Wein, A.J.; Rackley, R.R. Overactive bladder: A better understanding of pathophysiology, diagnosis, and management. *J. Urol.* **2006**, *175*, S5–S10.
5. Drake, M.J. The Overactive Bladder. In *Textbook of Female Urology and Urogynecology—Two-Volume Set*; CRC Press: Boca Raton, FL, USA, 2017; pp. 584–593.
6. Chapple, C.R.; Magera, A. Urgency incontinence and overactive bladder. In *Oxford Textbook of Urological Surgery*; Oxford University Press: Oxford, UK, 2017; pp. 282–288.
7. Dwyer, P.L.; Rosamilia, A. Evaluation and diagnosis of the overactive bladder. *Clin. Obstet. Gynecol.* **2002**, *45*, 193–204. [[CrossRef](#)] [[PubMed](#)]
8. Brown, J.S.; William, F.; McGhan, C.S. Comorbidities associated with overactive bladder. *Am. J. Manag. Care* **2000**, *6*, S574–S579. [[PubMed](#)]
9. Palma-Zamora, I.D.; Atiemo, H.O. Understanding the economic impact of neurogenic lower urinary tract dysfunction. *Urol. Clin.* **2017**, *44*, 333–343. [[CrossRef](#)] [[PubMed](#)]
10. Lin, K.-Y.; Siu, K.-C.; Lin, K.-H. Impact of lower urinary tract symptoms on work productivity in female workers: A systematic review and meta-analysis. *Neurourol. Urodyn.* **2018**, *37*, 2323–2334. [[CrossRef](#)] [[PubMed](#)]
11. Pierce, H.; Perry, L.; Chiarelli, P.; Gallagher, R. A systematic review of prevalence and impact of symptoms of pelvic floor dysfunction in identified workforce groups. *J. Adv. Nurs.* **2016**, *72*, 1718–1734. [[CrossRef](#)]
12. Chakraborty, B.J.; Crook, Drake, M.; Gilliland, N.; Gulur, D.; Kitney, D.; Manjunath, A.; Somov, P.; Vahabi, B. The Urinary Tract: Form and Function. In *Lower Urinary Tract Symptoms in Adults: A Clinical Approach*; Springer: Cham, Switzerland, 2020; pp. 1–17.
13. Kitney, D.G. Bladder Spontaneous Activity: Influence of Mild Heating and Inert Injectables. Ph.D. Dissertation, University of Surrey, Guildford, UK, 2016.
14. Bortolini, A.T.M.; Bilhar, A.P.M.; Castro, R.A. Neural control of lower urinary tract and targets for pharmacological therapy. *Int. Urogynecol. J.* **2014**, *25*, 1453–1462. [[CrossRef](#)]
15. Afrashteh, B. Identification of Lower Urinary Tract Dysfunction after Spinal Cord Injury at Lumbosacral Level by Developing a Clinical Relevance Rat Model. Ph.D. Dissertation, University of Salzburg, Salzburg, Austria, 2023.
16. Asl, S.O.K.Z. Analysis and Modeling of the Roles of Actin-Myosin Interactions in Bladder Smooth Muscle Biomechanics. Ph.D. Dissertation, Virginia Commonwealth University, Richmond, VA, USA, 2014.
17. Guntu, V.S.K. Biophysical Modeling to Reverse Engineer Two Mammalian Neural Circuits Lower Urinary Tract and Hippocampus. Ph.D. Dissertation, University of Missouri, Columbia, MO, USA, 2020.

18. Wyman, J.F.; Burgio, K.L.; Newman, D.K. Practical aspects of lifestyle modifications and behavioural interventions in the treatment of overactive bladder and urgency urinary incontinence. *Int. J. Clin. Pract.* **2009**, *63*, 1177–1191. [[CrossRef](#)]
19. Willis-Gray, M.G.; Alexis, A.D.; Elizabeth, J.G. Evaluation and management of overactive bladder: Strategies for optimizing care. *Res. Rep. Urol.* **2016**, *8*, 113–122. [[PubMed](#)]
20. Smith, L.E.; Rebecca, K.W.; Rubin, G.J. A systematic review of factors associated with side-effect expectations from medical interventions. *Health Expect.* **2020**, *23*, 731–758. [[CrossRef](#)] [[PubMed](#)]
21. Mostafaei, H.; Shariat, S.F.; Salehi-Pourmehr, H.; Janisch, F.; Mori, K.; Quhal, F.; Hajebrahami, S. The clinical pharmacology of the medical treatment for overactive bladder in adults. *Expert Rev. Clin. Pharmacol.* **2020**, *13*, 707–720. [[CrossRef](#)] [[PubMed](#)]
22. Hutchinson, A.; Nesbitt, A.; Joshi, A.; Clubb, A.; Perera, M. Overactive bladder syndrome: Management and treatment options. *Aust. J. Gen. Pract.* **2020**, *49*, 593–598. [[CrossRef](#)] [[PubMed](#)]
23. Fogaing, C.; Mossa, A.H.; Campeau, L. Are beta 3 adrenergic agonists now the preferred pharmacologic management of overactive bladder? *Curr. Urol. Rep.* **2020**, *21*, 1–12. [[CrossRef](#)] [[PubMed](#)]
24. Duong, V.; Iwamoto, A.; Pennycuff, J.; Kudish, B.; Iglesia, C. A systematic review of neurocognitive dysfunction with overactive bladder medications. *Int. Urogynecol. J.* **2021**, *32*, 2693–2702. [[CrossRef](#)] [[PubMed](#)]
25. Goodridge, S.D.; Rickey, L.M. Medical Therapy with Antimuscarinics and β 3-Agonists. In *Female Urinary Incontinence*; Springer International Publishing: Cham, Switzerland, 2022; pp. 147–164.
26. Drake, M.J.; Fry, C.H.; Hashitani, H.; Kirschner-Hermanns, R.; Rahnama, M.S.; Speich, J.E.; Tomoe, H.; Kanai, A.J.; McCloskey, K.D. What are the origins and relevance of spontaneous bladder contractions? ICI-RS 2017. *Neurourol. Urodyn.* **2018**, *37*, S13–S19. [[CrossRef](#)] [[PubMed](#)]
27. Mitsui, R.; Lee, K.; Uchiyama, A.; Hayakawa, S.; Kinoshita, F.; Kajioka, S.; Eto, M.; Hashitani, H. Contractile elements and their sympathetic regulations in the pig urinary bladder: A species and regional comparative study. *Cell Tissue Res.* **2020**, *379*, 373–387. [[CrossRef](#)]
28. Burdyga, T.V.; Wray, S. The relationship between the action potential, intracellular calcium and force in intact phasic, guinea-pig uretic smooth muscle. *J. Physiol.* **1999**, *520*, 867–883. [[CrossRef](#)]
29. Ter Keurs, H.E.D.J.; Boyden, P.A. Calcium and arrhythmogenesis. *Physiol. Rev.* **2007**, *87*, 457–506. [[CrossRef](#)]
30. Bolton, T.B.; Gordienko, D.V.; Pucovsky, V.; Parsons, S.; Povstyan, O. Calcium release events in excitation–contraction coupling in smooth muscle. In *Role of The Sarcoplasmic Reticulum in Smooth Muscle: Novartis Foundation Symposium 246*; John Wiley & Sons, Ltd.: Chichester, UK, 2002; Volume 246, pp. 154–173.
31. Sanders, K.M. Spontaneous electrical activity and rhythmicity in gastrointestinal smooth muscles. In *Smooth Muscle Spontaneous Activity: Physiological and Pathological Modulation*; Springer: Singapore, 2019; pp. 3–46.
32. Boopathi, E.; Gomes, C.; Zderic, S.A.; Malkowicz, B.; Chakrabarti, R.; Patel, D.P.; Wein, A.J.; Chacko, S. Mechanical stretch upregulates proteins involved in Ca^{2+} sensitization in urinary bladder smooth muscle hypertrophy. *Am. J. Physiol. Cell Physiol.* **2014**, *307*, C542–C553. [[CrossRef](#)] [[PubMed](#)]
33. Poley, R.N.; Dosier, C.R.; Speich, J.E.; Miner, A.S.; Ratz, P.H. Stimulated calcium entry and constitutive RhoA kinase activity cause stretch-induced detrusor contraction. *Eur. J. Pharmacol.* **2008**, *599*, 137–145. [[CrossRef](#)]
34. Kajioka, S.; Nakayama, S.; McMurray, G.; Abe, K.; Brading, A.F. Ca^{2+} channel properties in smooth muscle cells of the urinary bladder from pig and human. *Eur. J. Pharmacol.* **2002**, *443*, 19–29. [[CrossRef](#)]
35. Wu, C.; Sui, G.; Fry, C.H. The role of the L-type Ca^{2+} channel in refilling functional intracellular Ca^{2+} stores in guinea-pig detrusor smooth muscle. *J. Physiol.* **2002**, *538*, 357–369. [[CrossRef](#)] [[PubMed](#)]
36. Petkov, G.V. 14 Role of Ion Channels in Urinary Bladder Smooth Muscle Function. In *Signal Transduction and Smooth Muscle*; CRC Press: Boca Raton, FL, USA, 2018; p. 281.
37. Wray, S.; Burdyga, T. Sarcoplasmic reticulum function in smooth muscle. *Physiol. Rev.* **2010**, *90*, 113–178. [[CrossRef](#)]
38. Wu, C.; Fry, C.H. $\text{Na}^+/\text{Ca}^{2+}$ exchange and its role in intracellular Ca^{2+} regulation in guinea pig detrusor smooth muscle. *Am. J. Physiol. Cell Physiol.* **2001**, *280*, C1090–C1096. [[CrossRef](#)] [[PubMed](#)]
39. Herrera, G.M.; Nelson, M.T. Sarcoplasmic reticulum and membrane currents. In *Role of The Sarcoplasmic Reticulum in Smooth Muscle: Novartis Foundation Symposium 246*; John Wiley & Sons, Ltd.: Chichester, UK, 2002; Volume 246, pp. 189–207.
40. Provence, A. K_v7 Channels of the Urinary Bladder Smooth Muscle: Functional Roles and Therapeutic Potential. Ph.D. Thesis, University of South Carolina, Columbia, SC, USA, 2018.
41. Takagi, H.; Hashitani, H. Effects of K^+ channel openers on spontaneous action potentials in detrusor smooth muscle of the guinea-pig urinary bladder. *Eur. J. Pharmacol.* **2016**, *789*, 179–186. [[CrossRef](#)]
42. Hayase, M.; Hashitani, H.; Kohri, K.; Suzuki, H. Role of K^+ channels in regulating spontaneous activity in detrusor smooth muscle in situ in the mouse bladder. *J. Urol.* **2009**, *181*, 2355–2365. [[CrossRef](#)]
43. Xin, W.; Cheng, Q.; Soder, R.P.; Petkov, G.V. Inhibition of phosphodiesterases relaxes detrusor smooth muscle via activation of the large-conductance voltage- and Ca^{2+} -activated K^+ channel. *Am. J. Physiol. Cell Physiol.* **2012**, *302*, C1361–C1370. [[CrossRef](#)]
44. Hristov, K.L.; Parajuli, S.P.; Soder, R.P.; Cheng, Q.; Rovner, E.S.; Petkov, G.V. Suppression of human detrusor smooth muscle excitability and contractility via pharmacological activation of large conductance Ca^{2+} -activated channels. *Am. J. Physiol. Cell Physiol.* **2012**, *302*, C1632–C1641. [[CrossRef](#)]
45. Petkov, G.V. Role of potassium ion channels in detrusor smooth muscle function and dysfunction. *Nat. Rev. Urol.* **2012**, *9*, 30–40. [[CrossRef](#)] [[PubMed](#)]

46. Hristov, K.L.; Smith, A.C.; Parajuli, S.P.; Malysz, J.; Petkov, G.V. Large-conductance voltage- and Ca^{2+} -activated K^+ channel regulation by protein kinase C in guinea pig urinary bladder smooth muscle. *Am. J. Physiol. Cell Physiol.* **2014**, *306*, C460–C470. [[CrossRef](#)] [[PubMed](#)]
47. Parajuli, S.P.; Petkov, G.V. Activation of muscarinic M3 receptors inhibits large-conductance voltage- and Ca^{2+} -activated K^+ channels in rat urinary bladder smooth muscle cells. *Am. J. Physiol. Cell Physiol.* **2013**, *305*, C207–C214. [[CrossRef](#)] [[PubMed](#)]
48. Jenkins, D.P. *Modulators of Small and Intermediate Conductance Calcium-Activated Potassium Channel: Mechanism of Action and In Vivo Effects*; University of California: Davis, CA, USA, 2012.
49. Hristov, K.L.; Smith, A.C.; Parajuli, S.P.; Malysz, J.; Rovner, E.S.; Petkov, G.V. Novel regulatory mechanism in human urinary bladder: Central role of transient receptor potential melastatin 4 channels in detrusor smooth muscle function. *Am. J. Physiol. Cell Physiol.* **2016**, *310*, C600–C611. [[CrossRef](#)] [[PubMed](#)]
50. Hamilton, K.L. New life in overactive bladder. Focus on “Novel regulatory mechanism in human urinary bladder: Central role of transient receptor potential melastatin 4 channels in detrusor smooth muscle function”. *Am. J. Physiol. Cell Physiol.* **2016**, *310*, C597–C599. [[CrossRef](#)] [[PubMed](#)]
51. Smith, A.C.; Hristov, K.L.; Cheng, Q.; Xin, W.; Parajuli, S.P.; Earley, S.; Malysz, J.; Petkov, G.V. Novel role for the transient potential receptor melastatin 4 channel in guinea pig detrusor smooth muscle physiology. *Am. J. Physiol. Cell Physiol.* **2013**, *304*, C467–C477. [[CrossRef](#)] [[PubMed](#)]
52. Smith, A.C.; Parajuli, S.P.; Hristov, K.L.; Cheng, Q.; Soder, R.P.; Afeli, S.A.Y.; Earley, S.; Xin, W.; Malysz, J.; Petkov, G.V. TRPM4 channel: A new player in urinary bladder smooth muscle function in rats. *Am. J. Physiol. Ren. Physiol.* **2013**, *304*, F918–F929. [[CrossRef](#)] [[PubMed](#)]
53. Provence, A.; Rovner, E.S.; Petkov, G.V. Regulation of transient receptor potential melastatin 4 channel by sarcoplasmic reticulum inositol trisphosphate receptors: Role in human detrusor smooth muscle function. *Channels* **2017**, *11*, 459–466. [[CrossRef](#)] [[PubMed](#)]
54. Launay, P.; Fleig, A.; Perraud, A.-L.; Scharenberg, A.M.; Penner, R.; Kinet, J.-P. TRPM4 is a Ca^{2+} -activated nonselective cation channel mediating cell membrane depolarization. *Cell* **2002**, *109*, 397–407. [[CrossRef](#)]
55. Parajuli, S.P.; Hristov, K.L.; Sullivan, M.N.; Xin, W.; Smith, A.C.; Earley, S.; Malysz, J.; Petkov, G.V. Control of urinary bladder smooth muscle excitability by the TRPM4 channel modulator 9-phenanthrol. *Channels* **2013**, *7*, 537–540. [[CrossRef](#)]
56. Malysz, J.; Petkov, G.V. Urinary bladder smooth muscle ion channels: Expression, function, and regulation in health and disease. *Am. J. Physiol. Ren. Physiol.* **2020**, *319*, F257–F283. [[CrossRef](#)] [[PubMed](#)]
57. Hegde, S.S.; Eglén, R.M. Muscarinic receptor subtypes modulating smooth muscle contractility in the urinary bladder. *Life Sci.* **1999**, *64*, 419–428. [[CrossRef](#)] [[PubMed](#)]
58. Ehlert, F.J. Contractile role of M2 and M3 muscarinic receptors in gastrointestinal, airway and urinary bladder smooth muscle. *Life Sci.* **2003**, *74*, 355–366. [[CrossRef](#)] [[PubMed](#)]
59. Andersson, K.-E. Potential benefits of muscarinic M3 receptor selectivity. *Eur. Urol. Suppl.* **2002**, *1*, 23–28. [[CrossRef](#)]
60. Nausch, B.; Heppner, T.J.; Nelson, M.T. Nerve-released acetylcholine contracts urinary bladder smooth muscle by inducing action potentials independently of IP_3 -mediated calcium release. *Am. J. Physiol. -Regul. Integr. Comp. Physiol.* **2010**, *299*, R878–R888. [[CrossRef](#)] [[PubMed](#)]
61. Goïllard, J.-M.; Marder, E. Ion channel degeneracy, variability, and covariation in neuron and circuit resilience. *Annu. Rev. Neurosci.* **2021**, *44*, 335–357. [[CrossRef](#)] [[PubMed](#)]
62. Walpole, J.; Papin, J.A.; Peirce, S.M. Multiscale computational models of complex biological systems. *Annu. Rev. Biomed. Eng.* **2013**, *15*, 137–154. [[CrossRef](#)] [[PubMed](#)]
63. Aliev, R.R.; Richards, W.; Wikswo, J.P. A simple nonlinear model of electrical activity in the intestine. *J. Theor. Biol.* **2000**, *204*, 21–28. [[CrossRef](#)] [[PubMed](#)]
64. Bursztyn, L.; Eytan, O.; Jaffa, A.J.; Elad, D. Mathematical model of excitation-contraction in a uterine smooth muscle cell. *Am. J. Physiol. Cell Physiol.* **2007**, *292*, C1816–C1829. [[CrossRef](#)]
65. Tong, W.C.; Choi, C.Y.; Karche, S.; Holden, A.V.; Zhang, H.; Taggart, M.J. A computational model of the ionic currents, Ca^{2+} dynamics and action potentials underlying contraction of isolated uterine smooth muscle. *PLoS ONE* **2011**, *6*, e18685. [[CrossRef](#)]
66. Rihana, S.; Terrien, J.; Germain, G.; Marque, C. Mathematical modeling of electrical activity of uterine muscle cells. *Med. Biol. Eng. Comput.* **2009**, *47*, 665–675. [[CrossRef](#)] [[PubMed](#)]
67. Mahapatra, C. # 2696 In Silico Electrophysiological Study Reveals Tamsulosin Mediates Ureter Smooth Muscle Contraction by Increasing Potassium Current. *Nephrol. Dial. Transplant.* **2023**, *38* (Suppl. S1), gfad063c_2696.
68. Mahapatra, C.; Manchanda, R. Computational studies on ureter smooth muscle: Modeling ion channels and their role in generating electrical activity. In Proceedings of the 2019 Summer Simulation Conference, Berlin, Germany, 22–24 July 2019; pp. 1–6.
69. Mahapatra, C.; Pradhan, A. FC025: Physiological Role of KV Channel in Ureter Smooth Muscle Cell Investigated Quantitatively by Electrophysiological Modeling. *Nephrol. Dial. Transplant.* **2022**, *37* (Suppl. S3), gfac100-001. [[CrossRef](#)]
70. Poh, Y.C.; Corrias, A.; Cheng, N.; Buist, M.L. A quantitative model of human jejunal smooth muscle cell electrophysiology. *PLoS ONE* **2012**, *7*, e42385. [[CrossRef](#)] [[PubMed](#)]
71. Mahapatra, C.; Manchanda, R. In-Silico Investigation of Castration on Vas Deferens Smooth Muscle Electrophysiology. *FASEB J.* **2022**, *36*. [[CrossRef](#)]

72. Mahapatra, C.; Manchanda, R. Modeling Vas Deferens Smooth Muscle Electrophysiology: Role of Ion Channels in Generating Electrical Activity. In *Soft Computing for Problem Solving: SocProS 2017, Volume 2*; Springer: Singapore, 2019; pp. 655–663.
73. Mahapatra, C. Modulating Effects of Castration on vas Deferens Smooth Muscle Electrical Activities: Insights from a Quantitative study. *Fertil. Steril.* **2021**, *116*, e349. [[CrossRef](#)]
74. Mahapatra, C.; Manchanda, R. Modeling VAS Deferens Smooth Muscle Electrophysiology: Role of Ion Channels in Generating Electrical Activity. *Biophys. J.* **2020**, *118*, 259a–260a. [[CrossRef](#)]
75. Corrias, A.; Buist, M.L. A quantitative model of gastric smooth muscle cellular activation. *Ann. Biomed. Eng.* **2007**, *35*, 1595–1607. [[CrossRef](#)]
76. Corrias, A.; Buist, M.L. Quantitative cellular description of gastric slow wave activity. *Am. J. Physiol. Gastrointest. Liver Physiol.* **2008**, *294*, G989–G995. [[CrossRef](#)]
77. Kapela, A.; Bezerianos, A.; Tsoukias, N.M. A mathematical model of Ca²⁺ dynamics in rat mesenteric smooth muscle cell: Agonist and NO stimulation. *J. Theor. Biol.* **2008**, *253*, 238–260. [[CrossRef](#)]
78. Miftakhov, R.N.; Abdusheva, G.R.; Wingate, D.L. Model predictions of myoelectrical activity of the small bowel. *Biol. Cybern.* **1996**, *74*, 167–179. [[CrossRef](#)] [[PubMed](#)]
79. Mahapatra, C. Computational Study of Action Potential Generation in Urethral Smooth Muscle Cell. In Proceedings of the Computational Advances in Bio and Medical Sciences: 10th International Conference, ICCABS 2020, Virtual Event, 10–12 December 2020; Revised Selected Papers 10. Springer International Publishing: New, York, NY, USA, 2021; pp. 26–32.
80. Mahapatra, C.; Adam, S.; Gupta, A. Computational modeling of electrophysiological properties in urethral smooth muscle cell. *J. Comput. Neurosci.* **2021**, *49*, S81–S83.
81. Cha, C.Y.; Earm, K.H.; Youm, J.B.; Baek, E.B.; Kim, S.J.; Earm, Y.E. Electrophysiological modelling of pulmonary artery smooth muscle cells in the rabbits—Special consideration to the generation of hypoxic pulmonary vasoconstriction. *Prog. Biophys. Mol. Biol.* **2008**, *96*, 399–420. [[CrossRef](#)]
82. Mahapatra, C.; Samuilik, I. A Mathematical Model of Spontaneous Action Potential Based on Stochastics Synaptic Noise Dynamics in Non-Neural Cells. *Mathematics* **2024**, *12*, 1149. [[CrossRef](#)]
83. Mahapatra, C.; Brain, K.L.; Manchanda, R. A biophysically constrained computational model of the action potential of mouse urinary bladder smooth muscle. *PLoS ONE* **2018**, *13*, e0200712. [[CrossRef](#)]
84. Mahapatra, C.; Dave, V.; Manchanda, R. A Mathematical Modeling of Voltage-gated Calcium ion channel-based Calcium Transient Response in UrinaryBladder Smooth Muscle Cell. *Int. J. Pure Appl. Math.* **2017**, *117*, 71–75.
85. Mahapatra, C.; Manchanda, R. Simulation of In Vitro-Like Electrical Activities in Urinary Bladder Smooth Muscle Cells. *J. Biomim. Biomater. Biomed. Eng.* **2017**, *33*, 45–51. [[CrossRef](#)]
86. Mahapatra, C.; Manchanda, R. Modulating Properties of Hyperpolarization-Activated Cation Current in Urinary Bladder Smooth Muscle Excitability: A Simulation Study. In *Recent Findings in Intelligent Computing Techniques: Proceedings of the 5th ICACNI 2017, Volume 1*; Springer: Singapore, 2019; pp. 261–266.
87. Mahapatra, C.; Brain, K.L.; Manchanda, R. Computational study of Hodgkin-Huxley type calcium-dependent potassium current in urinary bladder over activity. In Proceedings of the 2018 IEEE 8th International Conference on Computational Advances in Bio and Medical Sciences (ICCABS), Las Vegas, NV, USA, 18–20 October 2018; IEEE: New, York, NY, USA; pp. 1–4.
88. Dave, V.; Mahapatra, C.; Manchanda, R. A mathematical model of the calcium transient in urinary bladder smooth muscle cells. In Proceedings of the 2015 37th Annual International Conference of the IEEE Engineering in Medicine and Biology Society (EMBC), Milan, Italy, 25–29 August 2015; IEEE: New, York, NY, USA, 2015; pp. 5359–5362.
89. Demion, M.; Bois, P.; Launay, P.; Guinamard, R. TRPM4, a Ca²⁺-activated nonselective cation channel in mouse sino-atrial node cells. *Cardiovasc. Res.* **2007**, *73*, 531–538. [[CrossRef](#)]
90. Marom, S.; Marder, E. A biophysical perspective on the resilience of neuronal excitability across timescales. *Nat. Rev. Neurosci.* **2023**, *24*, 640–652. [[CrossRef](#)]
91. Chow, K.-Y.; Wu, C.; Sui, G.P.; Fry, C.H. Role of the T-type Ca²⁺ current on the contractile performance of guinea pig detrusor smooth muscle. *Neurourol. Urodyn. Off. J. Int. Cont. Soc.* **2003**, *22*, 77–82. [[CrossRef](#)]
92. Jaggar, J.H.; Porter, V.A.; Lederer, W.J.; Nelson, M.T. Calcium sparks in smooth muscle. *Am. J. Physiol. -Cell Physiol.* **2000**, *278*, C235–C256. [[CrossRef](#)] [[PubMed](#)]
93. Hodgkin, A.L.; Huxley, A.F. A quantitative description of membrane current and its application to conduction and excitation in nerve. *J. Physiol.* **1952**, *117*, 500. [[CrossRef](#)] [[PubMed](#)]
94. Noble, D. A modification of the Hodgkin—Huxley equations applicable to Purkinje fibre action and pacemaker potentials. *J. Physiol.* **1962**, *160*, 317. [[CrossRef](#)] [[PubMed](#)]
95. Fry, C.H.; Cooklin, M.; Birns, J.; Mundy, A.R. Measurement of intercellular electrical coupling in guinea-pig detrusor smooth muscle. *J. Urol.* **1999**, *161*, 660–664. [[CrossRef](#)] [[PubMed](#)]
96. Geng, Y.; Magleby, K.L. Single-channel kinetics of BK (Slo1) channels. *Front. Physiol.* **2015**, *5*, 129016. [[CrossRef](#)] [[PubMed](#)]
97. Heeger, D. Synaptic Input. 2000. Available online: <https://www.cns.nyu.edu/~david/handouts/synapse.pdf> (accessed on 19 June 2024).
98. Hines, M.L.; Carnevale, N.T. The NEURON simulation environment. *Neural Comput.* **1997**, *9*, 1179–1209. [[CrossRef](#)] [[PubMed](#)]

-
99. Carnevale, T. Neuron simulation environment. *Scholarpedia* **2007**, *2*, 1378. [[CrossRef](#)]
 100. Spiess, A.-N.; Neumeyer, N. An evaluation of R² as an inadequate measure for nonlinear models in pharmacological and biochemical research: A Monte Carlo approach. *BMC Pharmacol.* **2010**, *10*, 1–11. [[CrossRef](#)]

Disclaimer/Publisher's Note: The statements, opinions and data contained in all publications are solely those of the individual author(s) and contributor(s) and not of MDPI and/or the editor(s). MDPI and/or the editor(s) disclaim responsibility for any injury to people or property resulting from any ideas, methods, instructions or products referred to in the content.